JOURNAL OF CATALYSIS 129, 238–256 (1991)

Transport-Enhanced α-Olefin Readsorption Pathways in Ru-Catalyzed Hydrocarbon Synthesis

ENRIQUE IGLESIA,[1] SEBASTIAN C. REYES, AND ROSTAM J. MADON[2]

Corporate Research Laboratories, Exxon Research and Engineering Company, Route 22 East, Annandale, New Jersey 08801

Received September 18, 1990; revised December 19, 1990

Residence time and cofeed studies show that olefins and paraffins are primary products in Ru-catalyzed hydrocarbon synthesis. Olefins readsorb and initiate surface chains that are indistinguishable from those formed directly from CO/H_2 and that continue to grow and ultimately desorb as higher molecular weight hydrocarbons. Transport-enhanced α-olefin readsorption leads to an increase in chain growth probability (α) and in paraffin content with increasing pore and bed residence time. Deviations from conventional (Flory) polymerization kinetics and the increasing paraffinic content of higher hydrocarbons are quantitatively described by transport effects on the residence time of intermediate olefins, without requiring the presence of several types of chain growth sites. Our transport-reaction model combines a description of diffusive and convective transport with a mechanistic kinetic model of olefin readsorption and of CO hydrogenation and chain growth. It quantitatively describes carbon number, site density, pellet size, and space velocity effects on hydrocarbon synthesis rate and product distribution. The model is consistent with the experimentally observed maximum C_{5+} selectivities at intermediate values of site density and pellet size. These intermediate values permit extensive readsorption of α-olefins without significant CO arrival transport limitations. © 1991 Academic Press, Inc.

1. INTRODUCTION

Hydrocarbon synthesis from CO and H_2 is a key step in integrated processes for the conversion of natural gas to liquid fuels (*1, 2*). Catalytic CO hydrogenation occurs at metal sites located within porous pellets that frequently contain liquid products at reaction conditions. Consequently, reactant and product diffusion is slow; they often control hydrocarbon synthesis rates and selectivity even in small catalyst pellets.

Here, we describe how diffusion-limited CO arrival leads to high effective H_2/CO ratios at catalytic sites and thus decreases the C_{5+} synthesis rate and selectivity. We also show that convection- and diffusion-limited removal of reactive products (olefins) enhances their secondary readsorption, and chain initiation and growth, thus leading to higher molecular weight hydrocarbon products. Product distributions seldom obey Flory kinetics (*3*). Deviations from Flory kinetics are commonly attributed to the presence of several types of chain growth sites on catalytic surfaces (*4–6*). However, secondary olefin readsorption also increases the chain growth probability (α) and the paraffin content in the products. Here, we propose that olefin transport rates decrease as molecular size increases, leading to an increasing chain growth probability (non-Flory distribution) and to a decreasing olefin to paraffin ratio as the carbon number of the product molecules increases.

2. BACKGROUND

2.1 Olefin Readsorption Pathways

Early studies recognized that olefins, paraffins, and oxygenates were present in hydrocarbon synthesis products (*1, 7*). The re-

[1] To whom correspondence should be addressed.
[2] Current address: Engelhard Corporation, Menlo Park, Edison, NJ 08818.

0021-9517/91 $3.00
Copyright © 1991 by Academic Press, Inc.
All rights of reproduction in any form reserved.

activity of olefins and their incorporation into reaction products were first reported by Smith *et al.* (*8*) on Fe catalysts. Herrington (*9*) first proposed that growing surface chains terminate by desorption as paraffins or olefins and that the latter could readsorb and thus reenter the chain growth pathways.

Later studies showed the details of the readsorption and chain initiation pathways by establishing the ^{14}C content of products formed from mixtures of labeled olefins and H_2/CO (*10–15*). These studies revealed extensive hydrogenation of the added olefin along with readsorption and chain growth; Hall *et al.* (*14*), however, demonstrated that the addition of H_2O, an indigenous product of CO hydrogenation, inhibits secondary olefin hydrogenation reactions. A recent theoretical analysis of chain growth suggests that olefin readsorption effectively decreases the net termination rate of surface chains by reversing the termination step (H abstraction) that leads to α-olefin products (*16*). Several authors have suggested that the increased extent of readsorption of higher olefins results from their greater solubility in synthesis liquids (*18–20*).

2.2 Non-Flory Hydrocarbon Synthesis Product Distributions

Pichler *et al.* (*10*) first reported deviations from Flory kinetics in hydrocarbon synthesis reactions; they describe an increase in chain growth probability (α) with increasing molecular size and suggest that the intrinsic olefin readsorption rate on Co sites is higher for larger olefins. Schulz and co-workers (*17, 18*) suggested that deviations from Flory kinetics occurred in the carbon number range where products started to exit the reactor in the liquid rather than the gas phase. Non-Flory product distributions have also been attributed to the presence of multiple growth sites with distinct chain growth probabilities (*4–6*). Later studies proposed that the higher solubility of larger olefins increases their reactor residence time and enhances their chances of undergoing secondary reactions (*19, 20*).

2.3 Transport Effects in Hydrocarbon Synthesis Reactions

In the absence of transport limitations, all components in the gas and liquid phases within a reacting system are in thermodynamic equilibrium; therefore, the presence of a liquid phase affects neither the residence time nor the kinetic driving force (fugacity or chemical potential) of any component. In the absence of concentration, fugacity, or chemical potential gradients (induced by transport limitations), the presence of a liquid phase does not influence secondary reactions. Here, we show that carbon number effects on α and on olefin content result from intraparticle diffusion limitations that increase the residence time and the fugacity of higher molecular weight products within liquid-filled pores. Similar effects are observed when α-olefin removal is limited by convective flow within packed-bed interstices.

Anderson *et al.* (*21*) first reported that intraparticle diffusional restrictions on the rate of reactant arrival to hydrocarbon synthesis sites controlled the CO conversion rate of Fe-based catalysts. Recently, Post *et al.* (*22*) report a simplified transport-reaction model that describes only H_2 transport limitations, although CO is the more probable diffusion-limited reactant, in Fe and Co catalysts; they address only rate effectiveness factors for the primary CO hydrogenation reaction and do not discuss transport effects on synthesis selectivity or on secondary reactions.

Here, we report a transport-reaction model of hydrocarbon synthesis selectivity that describes intraparticle (diffusion) and interparticle (convection) transport processes; these processes control the rate of arrival of CO and H_2 and the rate of removal of reactive products within catalyst pellets and reactors. The model is consistent with the observed effects of pore and bed residence time on hydrocarbon synthesis selectivity.

3. EXPERIMENTAL PROCEDURES

3.1 Catalyst Preparation

Catalysts were prepared by contacting calcined (air, 873 K, 4 h) TiO_2 (P25, Degussa, 60% rutile), SiO_2 (Davison, Grade 62), and γ-Al_2O_3 (Catapal SB) supports with a Ru nitrate (Engelhard)/acetone solution; the samples were dried by slow evaporation of the acetone solvent at room temperature followed by evacuation at 373 K. The catalysts were then reduced (H_2, 723 K, 4 h) and passivated; they were reduced again at 673 K before catalytic or chemisorption experiments. The unsupported Ru powder (Johnson-Mathey, Puratronic grade) was reduced using a similar procedure. Unless otherwise noted, the 80–140 mesh size fractions (0.17 mm average diameter) were used in all catalytic experiments.

3.2 Catalyst Characterization

Elemental compositions were determined by X-ray fluorescence and atomic absorption. Metal crystallite size distributions were calculated from electron microscopy and X-ray diffraction measurements. Support surface areas and pore size distributions were determined by N_2 physisorption at 77 K (*23*).

Ru dispersions, defined as the fraction of total Ru atoms residing at the surface of supported crystallites, was determined by titration of preadsorbed oxygen with dihydrogen at 373 K in a static chemisorption system. This technique accurately measures the density of surface Ru atoms even on TiO_2-supported samples, where metal-support interactions strongly inhibit dihydrogen chemisorption (*24*).

3.3 Catalytic Reaction Measurements

Steady-state kinetics and residence time and olefin cofeed effects were measured in an isothermal (±0.5 K) fixed-bed reactor at 476 K, 100–2000 kPa, and a stoichiometric H_2/CO ratio (2.1/1). The reactor effluent was analyzed directly (C_1–C_{15}, CO, CO_2, N_2) and after product collection (C_{16+}) by capillary and packed-column gas chromatography (FID, TCD, and MS detection). C_{35+} products were analyzed by high-temperature gel permeation chromatography using a refractive index detector. Reactant conversion and product selectivities were measured using dinitrogen as an internal standard.

We report selectivities on a carbon-atom basis as the percentage of the converted CO that appears as a given product. Hydrocarbon synthesis rates are reported both as Ru-normalized rates (metal-time yield; moles CO converted/g atom Ru · s) and as site-normalized rates (site-time yield; moles CO converted/g atom surface Ru · s). Space velocity is reported as the feed flow rate per total (not void) reactor volume. Residence time (space time) is defined as the reciprocal of space velocity.

3.4 Product Distribution Calculations

Mathematical treatments developed for polymerization kinetics are well-suited for the analysis of hydrocarbon synthesis products. When the growth probability (α) is independent of chain size, polymerization products are well described by the Flory equation [3a],

$$S_n = n(1 - \alpha)^2\alpha^{n-1}, \qquad (1)$$

where S_n is the fraction of the carbon atoms contained within chains with n carbons.

Hydrocarbon synthesis from H_2/CO requires the initiation of surface chains, their growth by addition of CH_x monomers, and their ultimate, and potentially reversible, termination by desorption from the surface as olefins, paraffins, and oxygenates (Scheme 1). Anderson (*25*) first used a relation,

$$\phi_n = \phi_i\alpha^{n-1}, \qquad (2)$$

that is readily obtained from Eq. (1), in order to describe hydrocarbon synthesis products.

In our treatment, we have chosen to describe the product distribution by calculating chain termination probabilities for each

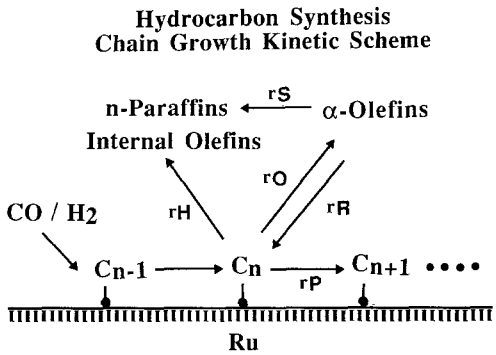

SCHEME 1

chain size, n, using (9):

$$\beta_{T,n} = \frac{r_{t,n}}{r_{p,n}} = \frac{\phi_n}{\sum_{i=n+1}^{\infty}\phi_i} . \qquad (3)$$

This approach is more rigorous and general than the Flory formalism but requires accurate measurements of the entire molecular weight distribution. The total termination probability, $\beta_{T,n}$, can be expressed as a linear combination of the individual termination pathways described in Scheme 1:

$$\beta_{T,n} = \beta_{0,n} + \beta_{H,n} - \beta_{r,n}. \qquad (4)$$

The total termination probability ($\beta_{T,n}$) decreases as the extent of readsorption ($\beta_{r,n}$) increases; the latter can be enhanced by increasing either the olefin reactivity (rate constant) or the olefin concentration within pellets and reactors.

The chain growth probability is given by

$$\alpha_n = \frac{1}{1+\beta_n} = \frac{\sum_{i=n+1}^{\infty}\phi_i}{\sum_{i=n}^{\infty}\phi_i} ; \qquad (5)$$

it is not a linear combination of the individual chain growth probabilities. When α_n is independent of n, Eq. (5) transforms to $\alpha = \phi_{n+1}/\phi_n$, from which Eq. (1) or its mole fraction analog are readily obtained. Note that the commonly reported semilogarithmic plots of S_n/n or ϕ_n vs n are only valid for the total product fraction within a given carbon number (S_n, ϕ_n) and give only the total chain growth probability (α); it is incorrect to use such plots to represent products of individual termination steps ($S_{n,p}$, $S_{n,0}$) or to estimate the individual chain growth probabilities (α_p, α_0).

4. RESULTS/DISCUSSION

4.1 Hydrocarbon Synthesis Rate and Selectivity on Ru Catalysts

Site-time yields were very similar ($1.1–2.2 \times 10^{-2}$ s^{-1}) on all Ru catalysts (Table 1). Support and dispersion effects appear minor for these materials at our reaction conditions. Selectivity differences actually arise from an effect of support physical structure on the extent of α-olefin readsorption, as we discuss in later sections. The kinetic rate expressions for CO hydrogenation and α-olefin readsorption were also very similar on all catalysts.

TABLE 1

Support Effects on Hydrocarbon Synthesis Rate and Selectivity

	1.2% wt Ru/TiO_2	10.8% wt Ru/SiO_2	5.0% wt Ru/Al_2O_3	Ru powder
Ru dispersion (%)	50	20	25	0.09
Ru time yield (s^{-1})	6.8×10^{-3}	2.3×10^{-3}	3.5×10^{-3}	2.0×10^{-5}
Site time yield (s^{-1})	1.3×10^{-2}	1.15×10^{-2}	1.4×10^{-2}	2.2×10^{-2}
Carbon selectivity (%)				
CH_4	3.7	4.2	5.0	2.0
C_2–C_4	9.0	6.7	7.0	2.8
C_{5+}	87.3	89.1	88.0	95

Note. 80–140 mesh (0.17-mm average diameter) pellets, 476–478 K, H_2/CO = 2.1, 600 kPa, 40–50% CO conversion; structural parameter, χ = 48–383, for all catalysts, see Section 4.6.

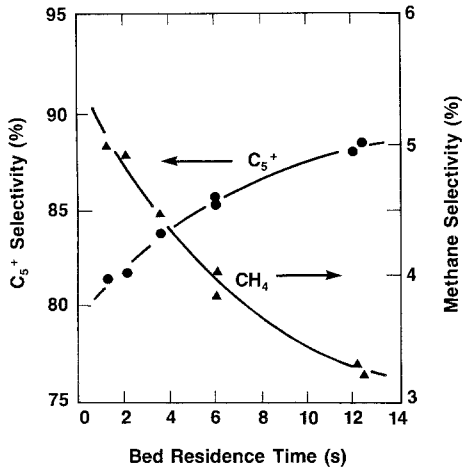

FIG. 1. Bed residence time effects on C_{5+} and CH_4 selectivity (1.2% wt Ru/TiO_2, 476 K, H_2/CO = 2.1, 600 kPa, 5–60% CO conversion).

4.2 Bed Residence Time Effects

The effect of bed residence time on hydrocarbon synthesis selectivity was examined by varying reactant space velocity at constant pressure and temperature. Bed residence time (τ_b) is defined here as the reciprocal of space velocity; it is proportional to the true residence time, which equals $\varepsilon_b \cdot \tau_b$ (ε_b is the bed void fraction ~0.36–0.40). The CO conversion level increases linearly with bed residence time up to about 60% CO conversion; the H_2/CO ratio remains independent of bed axial position or conversion because the feed and consumption ratios are identical.

Product molecular weight increases with increasing bed residence time. C_{5+} selectivity increases, while CH_4 selectivity decreases, as bed residence time and CO conversion increase on Ru/TiO_2 catalysts (Fig. 1). Product distributions are non-Flory at all bed residence times and show a distinct shift to higher molecular weight hydrocarbons as bed residence time increases (Fig. 2); the curvature of the distribution plots away from the abcissa is consistent with a chain growth probability that increases with chain size. The plots become linear for C_{25+} products; they reach an asymptotic α value (0.933) that is no longer dependent on bed residence time, carbon number, or the nature of the catalyst support. The asymptotic α values range from 0.93 to 0.945 for all catalysts studied. An increase in the chain growth probability of C_2–C_{25} hydrocarbons leads to the observed increase in molecular weight as bed residence time increases. These results suggest that secondary reactions lead to the net growth of light hydrocarbons.

The termination probability (β_T) of C_2–C_{25} surface chains is effectively reduced by increasing bed residence time or carbon number, whereas it remains unaffected by both for C_{25+} chains (Fig. 3). Moreover, β_T is unaffected by bed residence times below 2 s, values for which the removal of reactive products from the reactor by convective flow through interpellet voids is fast enough to prevent further secondary reactions after products exit catalyst pellets. Carbon number effects on β_T, however, remain even at short bed residence times, suggesting that the reactivity, concentration, or residence time of longer chains within pellets exceeds those of shorter ones.

These data suggest that secondary reactions allow reactive products to oligomerize or to reenter the chain growth pathways. The details of such readsorption pathways were determined by measuring the effect of

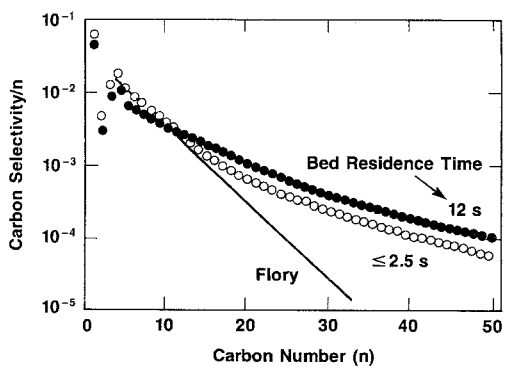

FIG. 2. Bed residence time effects on carbon number distributions (1.2% wt Ru/TiO_2, 476 K, H_2/CO = 2.1, 600 kPa, 5–60% CO conversion).

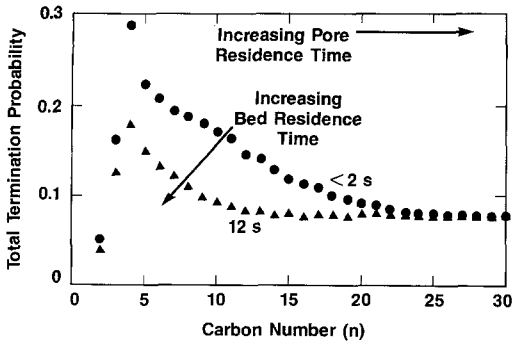

FIG. 3. Bed residence time and carbon number effects on total chain termination probability (1.2% wt Ru/TiO_2, 476 K, H_2/CO = 2.1, 600 kPa, 5–60% CO conversion).

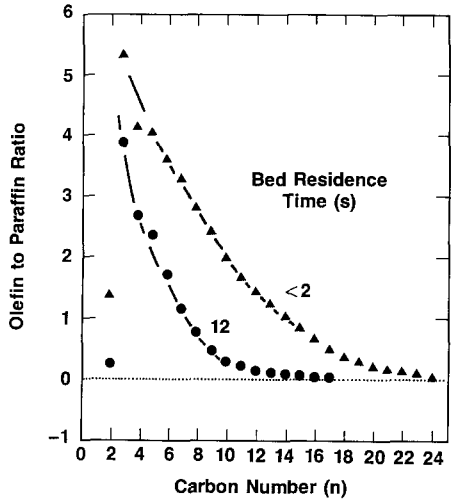

FIG. 4. Bed residence time and carbon number effects on α-olefin to n-paraffin ratio (1.2% wt Ru/TiO_2, 476 K, H_2/CO = 2.1, 600 kPa, 5–60% CO conversion; ▲, <2-s bed residence time, <8% CO conversion; ●, 12-s bed residence time, 60% CO conversion).

bed residence time on product functionality. The paraffin content in the product increases as bed residence time and carbon number increase (Fig. 4). Previous reports attributed these trends to secondary hydrogenation of primary α-olefin products (*15, 17*). Our data show that the increasing paraffin content arises predominantly from the net disappearance of light olefins and not from their direct hydrogenation to the corresponding n-paraffin (Fig. 5). Propylene selectivity decreases as we increase bed residence time without a corresponding increase in propane selectivity, leading to a net decrease in the fraction of the converted CO that appears as C_3 products (Fig. 5a). Similarly, 1-decene is selectively converted to C_{10+} products (Fig. 5b); the observed increase in n-decane and 2-decenes actually results from the combined effects of en-

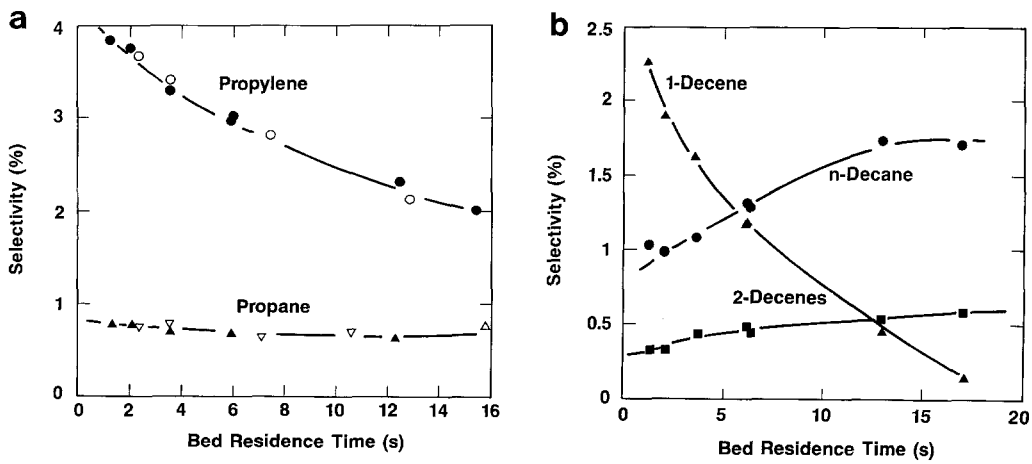

FIG. 5. Bed residence time effects on olefin and paraffin carbon selectivity. (a) C_3 products, (b) C_{10} products (1.2% wt Ru/TiO_2, 476 K, H_2/CO = 2.1, 600 kPa, 5–60% CO conversion).

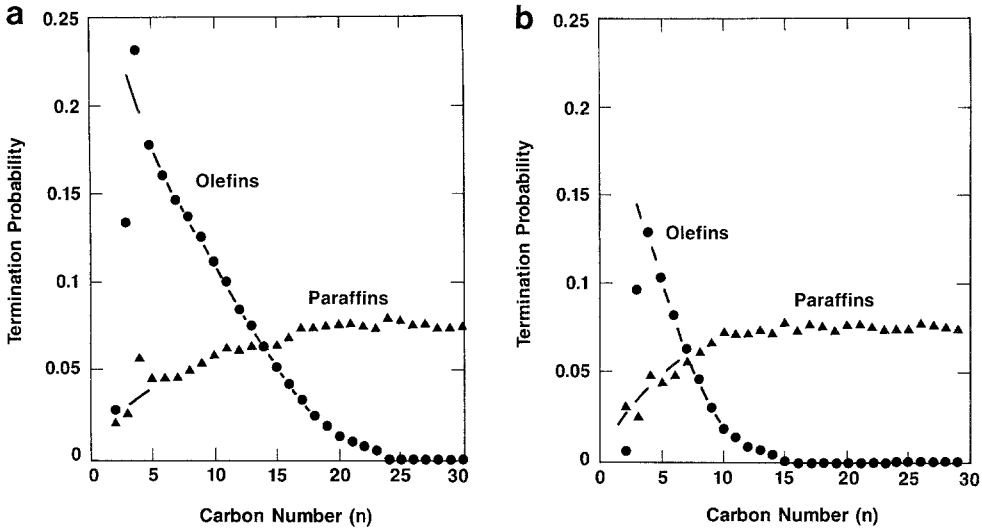

FIG. 6. Carbon number effects on olefin and paraffin chain termination probability (1.2% wt Ru/TiO_2, 476 K, H_2/CO = 2.1, 600 kPa, 5–60% CO conversion) (a) <2-s bed residence time, (b) 12-s bed residence time.

hanced readsorption of C_2–C_9 products as bed residence time increases. The fraction of converted CO that appears as C_{10} products is less affected by residence time than that of C_3 products because the net disappearance of 1-decene is partially offset by the higher concentration of surface C_{10} chains resulting from enhanced C_2–C_9 olefin readsorption. The details of these reaction pathways are discussed elsewhere (*26*).

We propose that selective α-olefin readsorption and chain initiation, rather than secondary hydrogenation, account for the observed effects of bed residence time on α-olefin to paraffin ratio. We also propose that α-olefin readsorption is enhanced by their slow removal from the reactor and that this accounts for the observed decrease in the termination probability of short chains as bed residence time increases. In effect, readsorption reverses a termination pathway for surface chains by allowing α-olefins to reenter the chain growth pathways.

The net probability of terminating surface chains as α-olefins ($\beta_{net} = \beta_0 - \beta_r$) decreases markedly with increasing bed residence and carbon number (Fig. 6); ultimately, such termination steps are totally reversed by readsorption and olefins no longer appear as gas-phase products. Then, the total termination probability (β_T) reaches an asymptotic value given by

$$\beta_{T,n} = \beta_{H,n}, \tag{6}$$

which is unaffected by further increases in bed residence time or carbon number. The probability of chain termination to *n*-paraffins (β_H) is insensitive to bed residence time and carbon number, as expected from the unreactive nature of *n*-paraffin products in hydrocarbon synthesis.

The methane chain termination probability is independent of bed residence time and much greater than the corresponding β_H for larger surface chains (0.51 vs 0.075) (Fig. 7a). Therefore, we conclude that the rate of H addition to surface methyl groups,

$$\beta_{H,1} = \frac{k_{H,1}(CH_3^*)(H^*)}{k_{p,1}(CH_3^*)(CH_x^*)} \qquad (* \text{ surface site}), \tag{7}$$

is favored over chain propagation to a much greater extent than for larger surface alkyls.

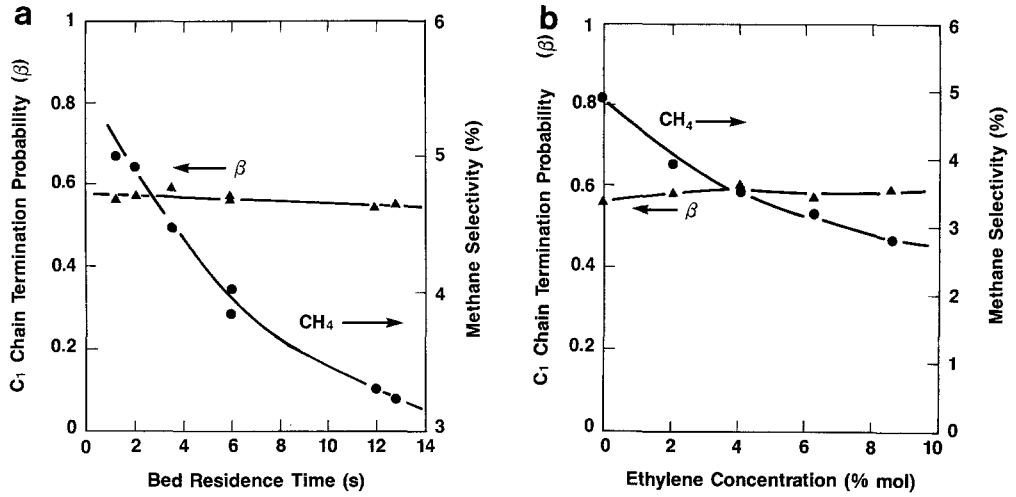

FIG. 7. Bed residence time and ethylene olefin cofeed effects on chain termination probability and methane carbon selectivity (1.2% wt Ru/TiO_2, 476 K, H_2/CO = 2.1, 600 kPa, 5–60% CO conversion) (a) bed residence time effects (5–65 CO conversion), (b) ethylene cofeed study (<8% CO conversion).

Moreover, these data suggest that the observed decrease in CH_4 selectivity as bed residence time increases arises from a decreased concentration of surface methyl chains because changes in surface monomer or hydrogen concentrations would lead to a similar decrease in β_{CH4}. Similar effects are observed when olefins are added to the H_2/CO feed (Fig. 7b), suggesting that olefins compete with surface methyls for available chain growth sites; in effect, monomers are added to longer chains, thus by-passing the C_1 chain initiators that are highly reactive in chain termination to CH_4 products.

4.3 Olefin Readsorption Studies

Olefin readsorption pathways were examined by the addition of C_2–C_{10} olefins (0.5–8% mol) to the H_2/CO feed. Olefin cofeed studies have previously shown the reactivity of α-olefins in chain initiation and growth, as well as their extensive conversion to the corresponding paraffin by secondary hydrogenation (*13–16*). The addition of α-olefins to the H_2/CO feed did not affect the rate of CO conversion; also, at low concentrations (<10% mol), added C_n α-olefins did not affect the chain growth probability of the C_{n+1} hydrocarbon synthesis product. These results suggest that α-olefins act primarily as chain initiators in Ru-catalyzed hydrocarbon synthesis.

Our bed residence time studies suggest that secondary olefin hydrogenation is a minor reaction compared with their selective readsorption and chain initiation and growth (Figs. 5 and 6). For example, more than 95% of the reacting ethylene and propylene molecules appear as longer chains while less than 5% appear as the hydrogenated product during hydrocarbon synthesis from CO/H_2 feeds (ethane or propane) (Table 2). External addition of these olefins, however, leads to much higher hydrogenation selectivities (~50%) (Table 2), in agreement with previous studies (*10–15*) but in clear disagreement with the results of our bed residence time studies.

The introduction of olefins below the reactor inlet significantly decreases the ethylene hydrogenation selectivity (50 to 22%, Table 2). The unique difference between added and indigenous (formed directly from H_2/CO) olefins in hydrocarbon synthesis is that the former probe the entire reactor bed while the latter contact only catalytic sites

TABLE 2

Ethylene Cofeed Studies

Source mol H_2O	Formed *in situ* from CO/H_2	6% Mol C_2H_4 added at reactor inlet	6% Mol C_2H_4 added below inlet[a]	6% Mol (C_2H_4 added at reactor inlet with 15% mol H_2O
% Chain initiation (to C_{3+})	>95[b]	50	76	89
% Hydrogenation (to C_2H_6)	<5[b]	50	22	11

Note. Ru/TiO_2, 476 K, H_2/CO = 2.1, 600 kPa (H_2 + CO) pressure, 18–22% CO conversion.

[a] At axial position z/H = 0.2, where H is total length of the reactor.

[b] From bed residence time studies.

below the point at which they are desorbed from a chain growth site. We propose that secondary hydrogenation of α-olefins occurs predominantly at conditions where the concentration of water, a product of the CO hydrogenation reaction, is low. Indeed, the addition of water along with ethylene to the H_2/CO feed results in C_{3+} selectivities that are very similar to those of indigenous ethylene (Table 2). We conclude that water (indigenous or added) inhibits the secondary hydrogenation of α-olefins during CO hydrogenation. Therefore, olefin cofeed studies at low pressure, low conversion, or by olefin introduction at the reactor inlet clearly underestimate the role of α-olefin readsorption and chain initiation and growth in steady-state hydrocarbon synthesis.

Similar cofeed studies using propylene and 1-octene showed that the effects of bypassing the reactor inlet or of added water were independent of olefin size. The addition of an olefin of size n (C_n) led to a decrease in the selectivity of C_{n-1} products, because of selective displacement of such surface chains with C_{n+} species. The isomeric distribution of $C_{(n+1)+}$ olefin and paraffin products formed from the added C_n olefin or directly from H_2/CO were identical; this suggests that surface chains initiated by readsorbed olefins are kinetically indistinguishable from those directly formed by hydrogenation of CO and subsequent chain growth. Internal olefins were significantly less reactive that α-olefins in chain initiation and secondary hydrogenation reactions. The reactivity of added α-olefins in chain initiation reactions increased in the order

$$\text{ethylene} \gg \text{propylene} \gtrsim \text{1-butene} \sim C_{5+}\ \alpha\text{-olefins}.$$

The higher reactivity of ethylene and propylene leads to concentrations of C_2 and C_3 products below the curved distribution plots that describe the C_{4+} products (Fig. 2) and to the low termination probabilities for C_2 and C_3 surface chains (Fig. 3).

4.4 Pore Residence Time (Carbon Number) Effects

Hydrocarbon synthesis on Ru catalysts leads to non-Flory product distributions; the chain growth probability (α) increases with increasing chain length (n) (Fig. 2), even at bed residence times (<2.5 s), where transport by convection is sufficiently fast that α-olefins exiting a liquid-filled catalyst pellet leave the reactor effectively unreacted. In other words, product distributions are non-Flory, even when convection no longer enhances the probability of α-olefin readsorption and selectivity is no longer affected by further decreases in bed residence time. In effect, readsorption occurs even in reactors that effectively behave as single pellets.

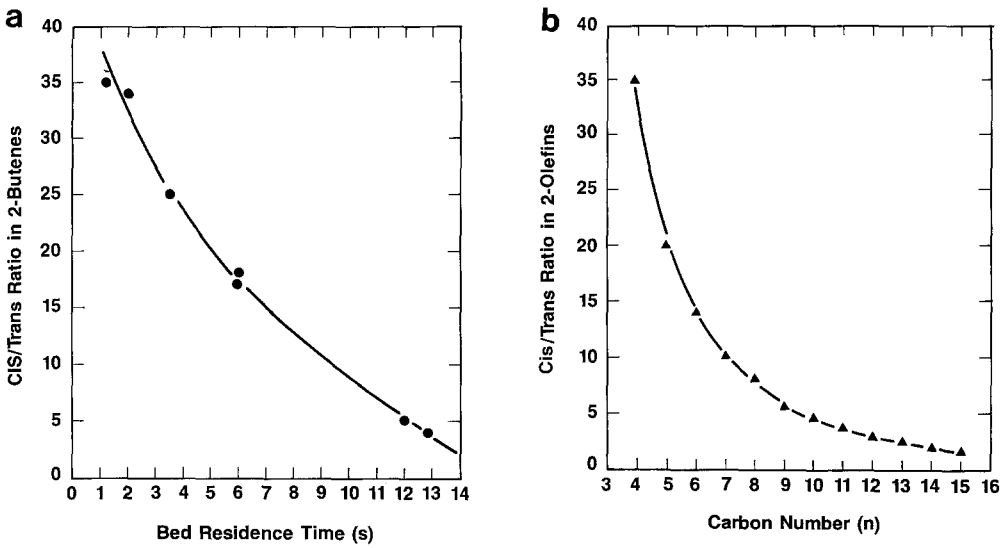

FIG. 8. Bed residence time and carbon number effects on *cis/trans*-2-olefin ratio (1.2% wt Ru/TiO_2, 476 K, 600 kPa, $H_2/CO = 2.1$) (a) bed residence time effects (2-butenes), (b) carbon number effects (<2.5-s bed residence time).

This section describes how the readsorption of reactive α-olefin products is enhanced by an increase in intrapellet residence time and concentration as their molecular size increases. An intraparticle (pore) diffusion restriction controls the olefin removal rate and prevents their equilibrium with the gas phase contained within interparticle voids; thus, it increases the effective olefin fugacity and their readsorption kinetic driving force within the liquid phase. The diffusional removal rate depends on carbon number in much the same way as convective removal depends on bed residence time. Indeed, carbon number and bed residence time have the same directional effect on hydrocarbon synthesis selectivity (α, β, paraffin content).

The chain termination probability (β_T) and the α-olefin/*n*-paraffin ratio decrease with increasing carbon number (Figs. 4 and 6) until α-olefins are totally consumed, at which point asymptotic values of β_T are obtained. The decrease in β_T with increasing carbon number arises exclusively from the gradual elimination of the olefin formation step (β_0) as a viable termination pathway (Fig. 6). Olefin (C_4–C_{10}) cofeed experiments suggest that the readsorption rate constants are independent of chain length for C_4 + α-olefins. In contrast, ethylene and propylene readsorption rate constants are higher than those for C_{4+} olefin. This results in the low β_T and β_0 observed for C_2 and C_3 products (Fig. 6) and in their appearance below the Flory curve that describes the C_{4+} products (Fig. 2). We propose that the enhanced readsorption of higher olefins arises from their lower diffusivity, longer residence time, and higher fugacity within liquid-filled pores, in other words, from diffusion-enhanced olefin readsorption.

Internal olefins appear as minor components among hydrocarbon synthesis products. Bed residence time and carbon number effects on their selectivity suggest that *cis*-internal olefins are primary reaction products; they undergo secondary *cis*- to *trans*-isomerization but no significant readsorption and chain growth or hydrogenation. Therefore the *cis/trans* isomer ratio in internal olefins decreases markedly with increasing bed residence time and carbon number (Fig. 8). Olefin cofeed studies show that the

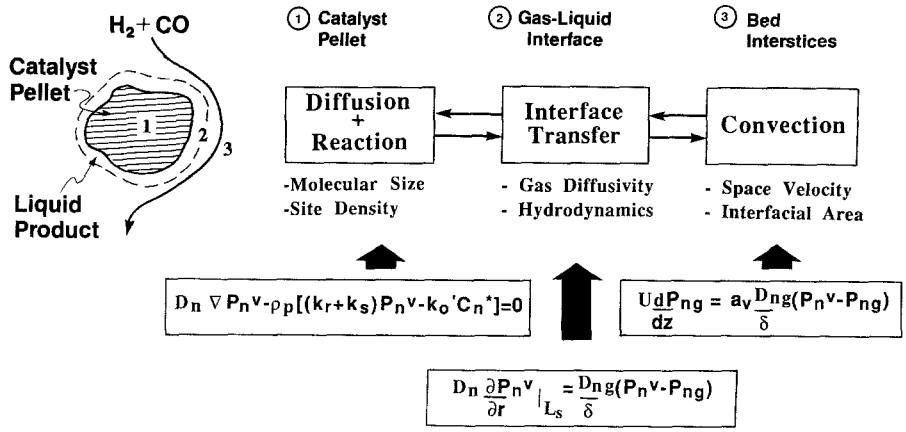

FIG. 9. Transport-enhanced α-olefin readsorption model.

secondary *cis–trans* isomerization rate depends on catalyst support

$$\gamma\text{-}Al_2O_3 > SiO_2 > TiO_2 > \text{Ru powder}$$

but that it is relatively insensitive to molecular size. Therefore, the extent of approach to equilibrium (equilibrium *cis/trans* = 0.5 at 476 K) provides an independent measure of olefin residence time on a given Ru catalyst. Figure 8 shows bed residence time effects on *cis/trans* ratios for a small olefin (2-butene) (Fig. 8a), as well as the approach to equilibrium by larger olefins at a very short bed residence time (<2 s) (Fig. 8b). *Cis/trans* ratios approach equilibrium values as we increase bed or pore (carbon number) residence time. These data show that the pore residence time of olefins (and of any hydrocarbon of similar size) increases markedly with molecular size. For example the *cis/trans* ratio difference between 2-butenes and 2-decenes is a factor of about 7 (35 vs 4.5); a similar change in the *cis/trans* ratio of 2-butenes requires a tenfold decrease in bed residence time (from 12.8 to 1.3 s).

The effects of bed and pore residence time on hydrocarbon synthesis selectivity are directionally similar; β_T, β_0, and α-olefin/*n*-paraffin ratio decrease with increasing bed residence time or carbon number, while β_H remains unchanged. Slower removal of α-olefins by convection (from bed interstices) or by diffusion (from intrapellet voids) enhances the extent to which readsorption occurs, resulting in the conversion of the α-olefins to higher molecular weight products, and in the effective reversal of the predominant chain termination (to olefin) pathway. The asymptotic chain termination probability (β_T) equals the intrinsic probability of chain termination to paraffins (β_H). These paraffins (and internal olefins) leave the catalyst pellets and the catalyst bed unreacted; thus they account for the majority of the product at long bed (high conversion) and pore (large chains) residence times.

4.5 Diffusion-Enhanced α-Olefin Readsorption Model

Readsorption enhancements caused by slow removal of olefins from the catalyst pores and from the bed interstices are described by the mathematical model shown schematically in Fig. 9. This model couples a chain growth kinetic model (Scheme 1) with diffusion and convection equations that describe transport processes in liquid-filled catalyst pellets and gas-phase bed interstices, respectively (Fig. 10). Surface reaction rate constants are assumed to be independent of chain length for C_{2+} surface chains. Readsorption rate constants are as-

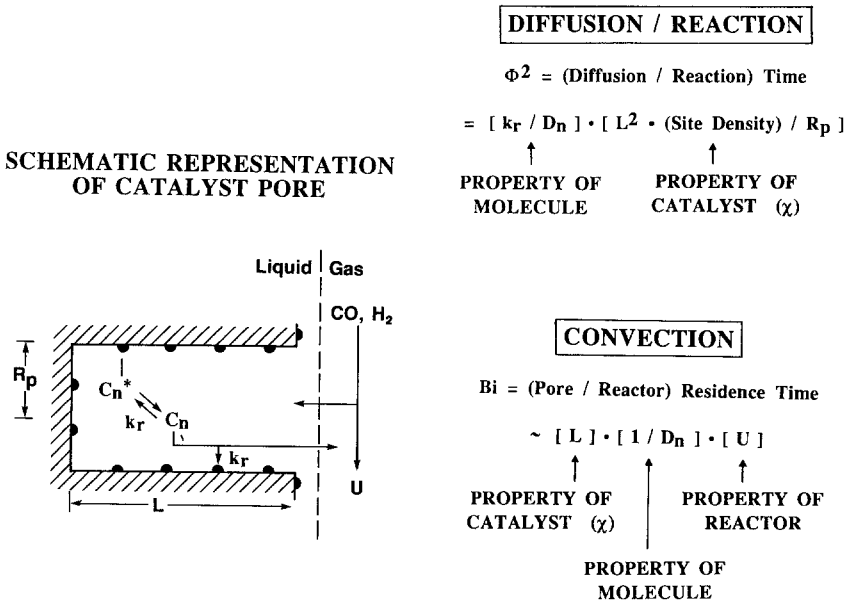

FIG. 10. Dimensional analysis of transport-enhanced α-olefin readsorption model.

sumed to be independent of chain length for C_{3+} α-olefins, higher for ethylene, and zero for non-terminal olefin species and for paraffins; thus, any carbon number effects on α or on product functionality arise exclusively from physical transport rather than chemical effects. We use the fugacity (or virtual pressure) of reactive species in the liquid phase, and not their liquid-phase concentration, as the kinetic driving force for the catalytic reaction. This approach is required by the transition state theory of chemical reaction kinetics (*27*); thus, in the absence of transport limitations, surface reactions are unaffected by the presence of a liquid phase that contains the reactants. The details of the model and the values of the required parameters in Figs. 11–15 are described in the Appendix.

Dimensional analysis of the coupled kinetic-transport equations suggest that a Thiele modulus (Φ) and a Biot number (Bi) describe diffusion and convection effects, respectively, on reactive processes (Fig. 10). The Thiele modulus,

$$\Phi_n^2 = \left(\frac{k_{r,n}}{D_n}\right)\left(\frac{L^2\theta_{Ru}}{R_p}\right), \qquad (8)$$

contains a term ($k_{r,n}/D_n$) that depends exclusively on the diffusing molecule and a χ term ($L^2\theta_{Ru}/R_p$) that includes structural catalyst parameters (Fig. 10). The first part introduces carbon number effects on selectivity; the second gives rise to pellet radius (L), pore radius (R_p), and site density (θ_{Ru}) effects on rates and selectivity as we change the physical properties of the Ru catalyst. The Biot number introduces a bed residence time effect (Fig. 10) on selectivity; it describes the relative effects of pore and bed residence on olefin readsorption probability.

A similar kinetic-transport model is used to describe the primary CO hydrogenation reaction. The details of the model are described elsewhere (*28*). The Thiele modulus for CO as the limiting reactant,

$$\Phi_{CO}^2 = \left(\frac{f(P_{CO}, P_{H_2})}{D_{CO}}\right) \cdot \left(\frac{L^2\theta_{Ru}}{R_p}\right) = \left(\frac{f(P_{CO}, P_{H_2})}{D_{CO}}\right) \cdot \chi, \qquad (9)$$

suggests a similar dependence of CO arrival and reactive α-olefin removal restrictions on catalyst structural properties.

The transport-enhanced readsorption

model was used to describe carbon number effects on chain termination probabilities and α-olefin/n-paraffin ratios. Input parameters to the model include a carbon number-dependent olefin diffusivity,

$$D_n = D_{n,0}e^{-0.3n}, \quad (10)$$

that resembles the strong dependence of D_n on carbon number observed in reptation and entanglement models of hydrocarbon diffusion in polymer melts (*29*). The experimentally observed readsorption probability is explicitly included.

$$\beta_{r,2} = 10 \cdot \beta_r, \quad (11a)$$

but all other intrinsic readsorption rates are assumed to be independent of carbon number,

$$\beta_{r,3} = \beta_{r,4} = \beta_{r,5} \ldots = \beta_{r,n} = \beta_r, \quad (11b)$$

where β_r is the readsorption probability for C_{3+} α-olefins.

The carbon number distribution of the hydrocarbon synthesis product and the chain termination probabilities (β_T, β_0, β_H)[3] are described accurately by the reaction-transport model of Fig. 10, using a carbon number-dependent Thiele modulus,

$$\Phi_n^2 = \Phi_0^2 e^{0.3n}. \quad (12)$$

The non-Flory product distribution and the decreasing net termination rate to α-olefins with increasing chain size then arise naturally and exclusively from the increased pore residence time and fugacity of the reactive olefins as their molecular weight increases (Figs. 11 and 12).

The model predicts that the removal of transport limitations ($\Phi_0 \rightarrow 0$) leads to an increase in chain termination probability (Fig. 13) and ultimately to a carbon number distribution consistent with Flory polymerization kinetics (Fig. 11, dashed line). A comparison of the kinetic-limited ($\Phi_0 = 0$, $\beta_T = 0.31$ and independent of n, <2-s bed residence time) with the experimental, transport-limited ($\Phi_0^2 = 1.5$, $\beta_T^\infty = 0.075$, 12-s bed residence time) carbon number distributions show that 93% of C_{21+} and 99.8%

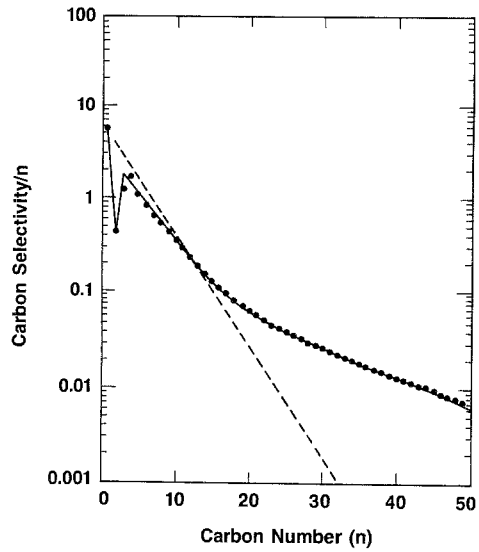

FIG. 11. Transport-enhanced α-olefin readsorption model. Carbon number distribution plots (1.2% wt Ru/TiO_2, 476 K, $H_2/CO = 2.1$, 600 kPa, 5–60% CO conversion range; ——, model predictions; ●, experimental data).

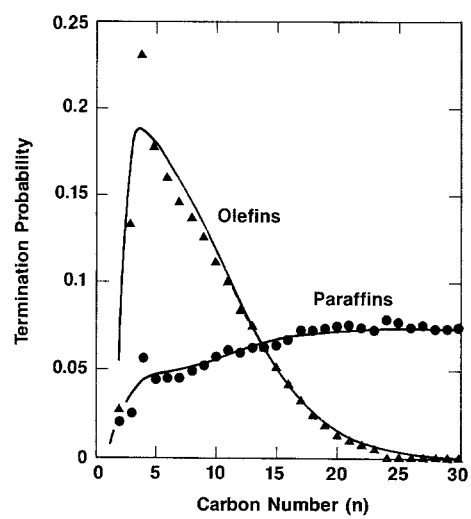

FIG. 12. Transport-enhanced α-olefin readsorption model. Chain termination probabilities (1.2% wt Ru/TiO_2, 476 K, $H_2/CO = 2.1$, 5–60% CO conversion; ——, model predictions; ▲●, experimental data).

[3] We have also included a secondary hydrogenation probability β_s in order to account for the slight increase in β as carbon number increases.

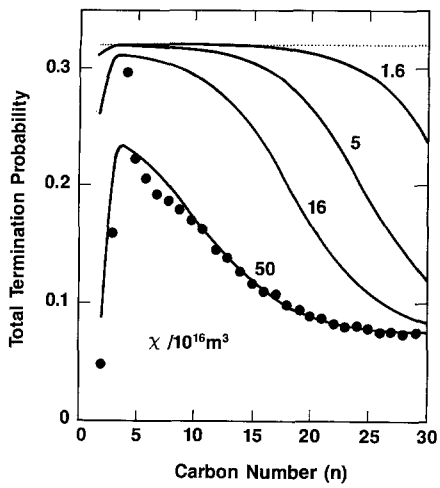

FIG. 13. Transport-enhanced α-olefin readsorption model. Carbon number and χ effects on chain termination probability (1.2% wt Ru/TiO_2, 476 K, H_2/CO = 2.1, 600 kPa, 5–60% CO conversion; ——, model predictions; ●, experimental data).

of the C_{41+} products require at least one readsorption event before their ultimate removal from catalyst pellets and reactor. Thus, the high wax (C_{20+}) selectivity typical of Ru catalysts depends largely on the ability of Ru sites to readsorb and continue to grow α-olefin molecules.

The removal of transport restrictions also leads to an α-olefin to n-paraffin ratio that is independent of chain length and that reflects the intrinsic chain termination probabilities of surface alkyl groups to α-olefins and n-paraffins. The model is also consistent with the experimentally observed values of α-olefin/n-paraffin ratio at short residence times (<2 s) and with the carbon number and bed residence time effects on paraffin content (Fig. 14).

4.6 Site Density and CO Transport Effects on Selectivity

The probability of readsorption increases as the intrinsic readsorption reactivity (k_r) of α-olefins and as their effective residence time in catalyst pores (τ_p) and bed interstices (τ_b) increase, as previously discussed and described in Fig. 9. In addition, the Thiele modulus (Eq. (8)) contains a parameter χ,

$$\chi = \frac{L^2\theta_{Ru}}{R_p}, \tag{13}$$

that contains exclusively structural properties of the support material (L, R_p) and the density of Ru sites (θ_{Ru}) that a diffusing α-olefin molecule encounters in exiting catalyst pores.

The C_{5+} selectivities at low CO conversion (<15%) on TiO_2-, Al_2O_3-, and SiO_2-supported Ru catalysts and on an unsupported Ru catalyst are shown in Fig. 15 and Table 3 as a function of the structural parameter χ, calculated from Eq. (13) and from the structural data in Table 3 and varied by changing the pellet radius (L), the average pore radius (R_p), and the Ru site density (θ_{Ru}). The C_{5+} selectivity initially increases with increasing χ, irrespective of the identity of the support or of the manner in which χ is varied. This increase in C_{5+} selectivity is accompanied by a decrease in the α-olefin/n-paraffin ratio and in the chain termination probability of light hydrocarbon chains (C_3–C_{15}) as χ increases. This structural parameter, however, does not affect the

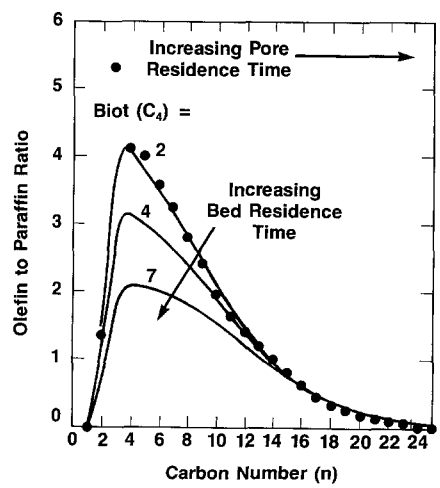

FIG. 14. Transport-enhanced α-olefin readsorption model. Bed residence time effects on α-olefin to n-paraffin ratios (Ru/TiO_2, 476 K, H_2/CO = 2.1, 600 kPa, 5–60% CO conversion; ——, model predictions; ●, experimental data).

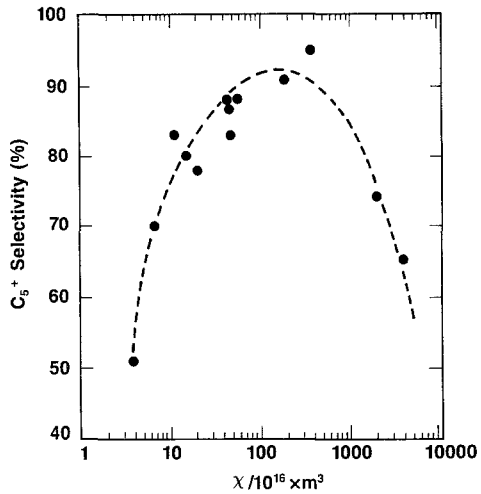

FIG. 15. Structural support and site density (χ) effects on C_{5+} selectivity (Ru catalysts, unsupported and on TiO_2, SiO_2, and γ-Al_2O_3 supports, 476 K, $H_2/CO = 2.1$, 600 kPa, <15% CO conversion; data from Table 3).

asymptotic value of β_T or β_H, suggesting that both are intrinsic properties of Ru sites, unaffected by transport limitations, and reflecting the intrinsic probability of chain termination to stable unreactive products.

These effects of structural parameters and of Ru site density are consistent with diffusion-enhanced readsorption of α-olefins. The ultimate decrease in C_{5+} selectivity at large values of χ results from the onset of transport limitations in the rate of conversion of reactants at catalytic sites. The diffusivity of CO in hydrocarbon synthesis wax is significantly higher than that of C_{3+} α-olefins; therefore, the onset of transport limitations occurs at larger and more reactive pellets (higher L, θ_{Ru}) for CO hydrogenation than for α-olefin readsorption. CO transport limitations lead to high effective hydrogen to carbon monoxide ratios at catalytic sites, which increase the chain termination probability (β_T, β_H) and the extent of secondary hydrogenation of α-olefins (β_s); leading to a lighter, more paraffinic product.

Our selectivity and rate data for catalysts with large χ values, as well as independent CO and H_2 diffusivity and solubility measurements, suggest that CO, and not H_2, is the diffusion-limited reactant for feeds with $H_2/CO > 1.6$. These results disagree with a previous proposal (*22*) that H_2 arrival rates control the rate of hydrocarbon synthesis on Co catalysts with kinetics and volumetric rates very similar to those on our Ru catalysts.

TABLE 3

Structural Parameters and Site Density Effects on the C_{5+} Selectivity of Ru Catalysts

Support (BET area m^2g^{-1})	% Wt Ru	% Ru dispersion	Average pellet radius $10^{-4} \times m$	Average pore radius $10^{-10} \times m$	Ru site density $10^{+16} \cdot m^{-2}$	χ $10^{+16} \cdot m^3$	C_{5+} Selectivity (%)
SiO_2 (280)	1.6	10	0.85	65	3.4	3.8	51
SiO_2(280)	10.8	20	0.85	65	45.1	50.4	87
TiO_2 (35)	1.2	50	0.85	150	102.1	49.2	83
TiO_2 (35)	0.4	50	0.85	150	34.1	16.4	80
TiO_2 (50)	1.04	45	7.0	135	55.8	202.5	74
None (0.07)	100	0.09	0.10	20	7660	383	95
γ-Al_2O_3 (280)	5.0	25	0.85	40	26.6	48.0	88
γ-Al_2O_3 (175)	1.1	30	0.85	40	11.3	20.4	78
TiO_2 (40)	0.3	50	0.85	135	22.4	12.0	83
TiO_2 (40)	2.5	30	0.85	135	112	60	88
TiO_2 (40)	0.3	30	0.85	135	13.4	7.1	70
TiO_2 (35)	1.2	50	1.80	150	102.1	210	91
TiO_2 (35)	1.2	50	7.5	150	102.1	3950	65

Note. 476–483 K, 600 kPa, $H_2/CO = 2.1$, <15% CO conversion.

4.7 Non-Flory Distributions and Transport Effects on Fe- and Co-Catalyzed Hydrocarbon Synthesis

Carbon number effects on chain growth probability and olefin content also occur on Fe- and Co-based hydrocarbon synthesis catalysts. In general, carbon number effects on α-olefin to paraffin ratio and the curvature of Flory plots increase in the order (*10–15*)

$$\text{Co} > \text{Ru} > \text{Fe},$$

reflecting the relative rates of olefin readsorption and chain initiation on these metals. The extension of our diffusion-enhanced readsorption model to Fe and Co catalysts is discussed elsewhere (*28*).

5. CONCLUSIONS

Residence time and olefin cofeed studies suggest that olefins and paraffins are primary hydrocarbon synthesis products. α-Olefins readsorb and initiate surface chains that are indistinguishable from those formed directly from CO and H_2 and that ultimately desorb as longer hydrocarbon chains. Secondary α-olefin hydrogenation is inhibited by the water formed during CO hydrogenation.

Olefin readsorption effectively reverses the chain termination step that leads to olefin products. Consequently, readsorption decreases the total chain termination probability (β_T) and the olefin content in the product. Slow removal of α-olefins from catalyst pores by diffusive processes, and from bed interstices by convective processes, increases the extent of readsorption. Therefore, chain termination probability and olefin content in the product decrease with increasing bed and pore residence time. Transport-enhanced α-olefin readsorption accounts for the non-Flory distribution of paraffinic products on Ru catalysts and for the increased C_{5+} selectivity as bed residence time and Ru site density increase.

Our transport-reaction model of α-olefin readsorption processes combines diffusive and convective transport processes with an intrinsic kinetic model of chain growth and termination. Catalyst pellet (diffusion) and reactor (convection) equations describe CO arrival and olefin removal effects on reaction selectivity. Thiele moduli and Biot numbers define the relative contributions of transport and reaction processes to reaction selectivity. Deviations from normal molecular weight distributions (non-Flory kinetics) and product functionality changes with carbon number are described for the first time by our pellet model; olefin pore residence time and fugacity increase with carbon number leading to enhanced secondary reactions and thus to higher chain growth probability and paraffin content in the higher molecular weight fractions. The reactor model describes the observed effects of bed residence time on carbon number and olefin distributions.

The combined CO arrival and olefin removal models predict an initial increase in product molecular weight with increasing site density and pellet size because of diffusion-enhanced olefin readsorption, followed by a decrease in molecular size as CO arrival becomes diffusion-limited. Therefore, maximum C_{5+} selectivities are obtained at intermediate values of site density and pellet size. Ruthenium catalyst formulations with such intermediate values were prepared and indeed found to exhibit optimum C_{5+} selectivity. The overall model describes the observed effects of space velocity, olefin recycle, pellet size, and pore structure on chain growth kinetics. Our study illustrates the crucial role of secondary reactions and of physical transport in hydrocarbon synthesis selectivity. It also suggests novel ways of controlling this selectivity by variations in catalyst pore structure and metal site density and by the incorporation of additional catalytic functionalities that effectively catalyze secondary pathways of primary hydrocarbon synthesis products.

APPENDIX

Here, we describe the complete set of equations and define all required parameters used in our simulations. In effect, we develop mass conservation equations for reactive (α-olefins) and unreactive (paraffins) products within a spherical catalyst pellet. The external boundary condition at the pellet surface couples the pellet equations with the corresponding material balances for α-olefins and paraffins in the interparticle voids within the packed bed.

The kinetic pathways described in Scheme 1, along with steady-state conservation of chain growth sites on the catalytic surface, require that

$$O = -k_p C_1^* C_n^* + k_p C_1^* C_{n-1}^* - k_o C_n^* - k_h C_n^* + k_r P_n^v/RT. \quad (A1)$$

Similarly, steady-state mass conservation equations for olefins and paraffins within interparticle voids are

$$O = D_n \nabla P_n^v - \rho_p[(k_r + k_s)P_n^v - k_o C_n^*] \quad \text{(olefins)} \quad (A2)$$

$$O = D_n \nabla Q_n^v + \rho_p[k_h C_n^* + k_s P_n^v] \quad \text{(paraffins);} \quad (A3)$$

here, we assume that olefins and paraffins of a given size have identical liquid-phase diffusivities. These equations (A2, A3) are subject to boundary conditions reflecting zero flux at the pellet center (i.e., symmetry condition) and balanced mass fluxes at the pellet surface between the pellet equations and the reactor gas-phase equations. The latter implies that

$$U\frac{dP_n^v}{dz} = a_v \frac{D_{ng}}{\delta}(P_n^v - P_{ng}) \quad (A4)$$

and

$$U\frac{dQ_n^v}{dz} = a_v \frac{D_{ng}}{\delta}(Q_n^v - Q_{ng}). \quad (A5)$$

The system of equations described above can be conveniently expressed in dimensionless form by defining

$$X_n = \frac{C_n^*}{C_0^*};\ Y_n = \frac{P_n^v}{P_{n|0}^v};\ Z_n = \frac{Q_n^v}{P_{n|0}^v};\ E_n = \frac{D_n}{D_{n,0}}$$

$$y_n = \frac{P_{ng}}{P_{ng|0}};\ z_n = \frac{Q_{ng}}{P_{ng|0}};\ e = \frac{D_{ng}}{D_{ng,0}}$$

$$\beta_0 = \frac{k_o}{k_p C_1^*};\ \beta_h = \frac{k_h}{k_p C_1^*};$$

$$\beta_r = \frac{k_r P_{n|0}^v}{k_p C_1^* C_0^*};\ \beta_s = \frac{k_s P_{n|0}^v}{k_p C_1^* C_0^*}$$

$$\xi = \frac{r}{L_s};\ \lambda = \frac{z}{H};$$

$$\Omega^2 = \frac{\rho_p L_s^2 k_p C_1^* C_0^*}{D_{n,0} P_{n|0}^v};\ \mathrm{Bi} = \frac{a_v D_{ng,0} H}{U\delta}.$$

These dimensionless parameters can be then substituted into Eqs. (A1)–(A5) to give

$$0 = X_{n-1} - (1 + \beta_0 + \beta_h)X_n + \beta_r Y_n \quad (A6)$$

$$0 = E_n \nabla Y_n - \Omega^2[(\beta_r + \beta_s)Y_n - \beta_0 X_n] \quad (A7)$$

$$0 = E_n \nabla Z_n + \Omega^2[\beta_n X_n + \beta_s Y_n] \quad (A8)$$

$$\frac{dy_n}{d\lambda} = e_n \mathrm{Bi}(Y_n - y_n) \quad (A9)$$

$$\frac{dz_n}{d\lambda} = e_n \mathrm{Bi}(Z_n - z_n). \quad (A10)$$

Substituting the recursive equation for X_n (A6) into Eq. (A7) allows us to define an effective Thiele modulus

$$\Phi_n^2 = \frac{\Omega^2}{E_n}\left(\beta_r + \beta_s - \frac{\beta_0\beta_r}{1 + \beta_0 + \beta_h}\right). \quad (A11)$$

This expression reduces to Eq. (8) in the text for the special case of no secondary hydrogenation ($\beta_s = 0$) and low termination probabilities ($\beta_0 \ll 1$), if we assume that the surface area per volume (s) is given by the usual expression for random assemblages of microspheres within support pellets,

$$s = \frac{2\phi}{R_p} \quad (A12)$$

and if the Ru site density is given by

$$\theta_{Ru} = \frac{2C_0^* \rho_p \phi}{R_p}. \qquad \text{(A13)}$$

The more complex Thiele modulus given by Eq. (A11), and actually used in our calculations, can also be separated into a part (χ) that depends exclusively on structural catalyst properties and another term that reflects the readsorption rate, the liquid diffusivity, and the reaction conditions.

These equations identify the key parameters used in the numerical solution of our kinetic-transport model. The parameter Ω^2 was kept at a value of 2.0, except in Fig. 13, where it was intentionally varied to explore the effect of catalyst structure on product selectivity. This value is consistent with experimental values of the parameters contained in the equation defining Ω. Diffusivities in the liquid (E_n) and gas phase (e_n) are assumed to be proportional to $e^{-0.3n}$ and $n^{-1/2}$, respectively. Biot numbers were calculated from experimental space velocity values. Chain termination probabilities (β_0, β_n, β_r, and β_s) were kept constant in all simulations; their values (0.29, 0.03, 0.40, and 0.08) were chosen in order to describe the behavior of C_4 hydrocarbons. The readsorption probability of ethylene ($\beta_{r,2}$) was chosen as 4.0, in agreement with experimental values obtained in ethylene cofeed experiments.

Equations (A6)–(A10) were solved recursively for every carbon number. The pellet equations were solved using orthogonal collocation on finite elements (*30*). The reactor equations were integrated using EPISODE subroutines (*31*).

NOMENCLATURE

a_v Bed interfacial area
Bi Biot number for interphase mass transfer
C_n Surface concentration of growing chains
D_n Hydrocarbon diffusivities in liquid-filled pores
$D_{n,0}$ Reference liquid diffusivity
D_{CO} CO diffusivity in liquid-filled pores
D_{ng} Hydrocarbon diffusivity in reactor gas phase
H Reactor length
i Carbon number
k_{CO} Rate constant of CO consumption
$k_{H,n}$ Termination rate constant
$k_{0,n}$ Rate constant for termination to *n*-olefin
$k_{p,n}$ Propagation rate constant
$k_{r,n}$ Readsorption rate constant
$k_{s,n}$ Secondary hydrogenation rate constant
n Carbon number
L Pellet radius
L_s Pellet surface
P_{CO} CO partial pressure
P_{ng} Olefin partial pressure on reactor gas phase
P_n^v Olefin virtual pressure in liquid phase
r_H Rate of termination to internal olefins
r_0 Rate of termination to α-olefins
r_r Rate of readsorption
r_s Rate of secondary hydrogenation
R_p Average pore radius
$r_{p,n}$ Propagation rate
$r_{t,n}$ Termination rate
S_n Fraction of carbon atoms in chains with n carbons
U Superficial gas velocity
z Axial reactor position
X_n Dimensionless concentration of surface chains of size n
Y_n Dimensionless virtual pressure of olefins in liquid
Z_n Dimensionless virtual pressure of paraffins in liquid
y_n Dimensionless gas-phase olefin concentration
z_n Dimensionless gas-phase paraffin concentration.

Greek Symbols

α_n Chain growth probability
$\beta_{H,n}$ Probability of chain termination to *n*-paraffins
$\beta_{0,n}$ Probability of chain termination to α-olefins

$\beta_{r,n}$	Readsorption probability
$\beta_{s,n}$	Probability of secondary hydrogenation of α-olefins
$\beta_{T,n}$	Total chain termination probability
δ	Boundary layer thickness
ε	Bed void fraction
θ_{Ru}	Ru site density (sites/m^2)
λ	Dimensionless reactor position
ξ	Dimensionless pellet position
ρ	Catalyst pellet density
τ_b	Bed residence time
τ_p	Pore residence time
ϕ	Mole fraction
Φ_n	Thiele modulus
$\Phi_{n,0}$	Reference Thiele modulus
χ	Structural parameter defined in Eq. (13)

ACKNOWLEDGMENTS

We thank Drs. G. D. Dupre and W. W. Schulz for their pioneering contributions to the analysis of hydrocarbon synthesis products by gas chromatography and gel permeation chromatography. We also gratefully acknowledge helpful discussions with Drs. S. L. Soled and R. A. Fiato during the course of this work.

REFERENCES

1. Pichler, H., *in* "Advances in Catalysis and Related Subjects" W. G. Frankenburg, V. I. Komarewsky, and E. K. Rideal, Eds.), Vol. 4, p. 271. Academic Press, New York, 1952.
2. Dry, M. E., *in* "Catalysis-Science and Technology" (J. R. Anderson and M. Boudart, Eds.) Vol. 1, p. 231–233. Springer-Verlag, Berlin, 1981.
3. (a) Flory, P. J., *J. Am. Chem. Soc.* **58,** 1877 (1936); (b) Friedel, R. A., and Anderson, R. B., *J. Am. Chem. Soc.* **72,** 1212 (1950); **72,** 2307 (1950).
4. Madon, R. J., and Taylor, W. F., *J. Catal.* **69,** 32 (1981).
5. Huff, G. A., and Satterfield, C. N., *J. Catal.* **85,** 370 (1984).
6. König, L., and Gaube, J., *Chem. Ing. Tech.* **55,** 14 (1983).
7. Fischer, F., and Tropsch, H., *Gesammelte Abh. Kennt. Kohle* **10,** 313 (1928).
8. Smith, D. L., Hawk, C. O., and Golden, P. L., *J. Am. Chem. Soc.* **52,** 3221 (1930).
9. Herrington, E. F., *Chem. Ind.* 347 (1946).
10. Pichler, H., Schulz, H., and Elstner, M., *Brennst. Chem.* **48,** 78 (1967).
11. Kolbel, H., and Ruschenburg, E., *Brennst. Chem.* **35,** 161 (1954).
12. Golovian, O. A., Sakharov, M. M., Roginsky, S. Z., and Dokukina, E., *Russ. J. Phys. Chem.* **33,** 471 (1959).
13. Roginsky, S. Z., *in* "Proceedings, 3rd International Congress Catalysis, Amsterdam, 1964," p. 939. Wiley, New York, 1965.
14. Hall, W. K., Kokes, R. J., and Emmett, P. H., *J. Am. Chem. Soc.* **82,** 1027 (1960).
15. Schulz, H., Rao, B. R., and Elstner, M., *Erdoel Kohle* **23,** 651 (1970).
16. Novak, S., Madon, R. J., and Suhl, H., *J. Catal.* **77,** 141 (1982).
17. Schulz, H., *Izv. Khim.* **17,** 3 (1984).
18. Schulz, H., Beck, K., and Erich, E., *in* "Proceedings, 9th International Congress on Catalysis, Calgary, 1988" (M. J. Phillips and M. Ternan, Eds.), Vol. 2, pp. 829–836. Chem. Inst. of Canada, Ottawa, 1988.
19. Vanhove, D., *Proc. Int. Meet. Soc. Fr. Chim., Div. Chim. Phys.*, 147 (1988).
20. Tau, L. M., Dabbagh, H. A., and Davis, B. H., *Energy Fuels* **4,** 94 (1990).
21. Anderson, R. B., Seligman, B., Schultz, J. F., Kelly, R. E., and Elliot, M. A., *Ind. Eng. Chem.* **44,** 391 (1952).
22. Post, M. F. M., van't Hoog, A. C., Minderhoud, J. K., and Sie, S. T., *AIChE J.* **35,** 1107 (1989).
23. Smith, J. M., "Chemical Engineering Kinetics," 3rd ed. McGraw-Hill, New York, 1981.
24. Iglesia, E., unpublished results.
25. Anderson, R. B., *in* "Catalysis" (P. H. Emmett, Ed.), Vol. IV. Rheinhold, New York, 1956.
26. Madon, R. J., Reyes, S. C., and Iglesia, E., submitted for publication.
27. Boudart, M., and Djega-Mariadassou, G., "Kinetics of Heterogeneous Catalytic Reactions." Princeton Univ. Press, Princeton, NJ, 1984.
28. Reyes, S. C., Iglesia, E., and Madon, R. J., in preparation.
29. DeGennes, P., *J. Chem. Phys.* **55,** 572 (1971); Bueche, F., "Physical Properties of Polymers." Interscience, London, 1962.
30. Carey, G. G. and Finlayson, B. A., *Chem. Eng. Sci.* **30,** 587 (1975).
31. Hindmarsh, A. C. and Byrne, G. D., EPISODE, Report UCID-30112, Lawrence Livermore Laboratory, 1985.